Penerbit Akademia Baru

Malaysian Journal on Composites Science and Manufacturing

Journal homepage:
https://www.akademiabaru.com/submit/index.php/mjcsm/
ISSN: 2716-6945

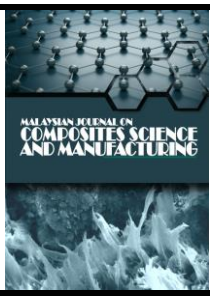


# Modeling Microstructural and Mechanical Properties of Solidified Al-Sn-Cu System

Open Access

Mahin Muntasir[1], Razia Khan Sharme[1,*], Mohammad Borhan Uddin[1], Mohammad Salman Haque[1], Fahim Khan[2]

[1] Department of Materials Science and Engineering, Khulna University of Engineering & Technology, Khulna-9203, Bangladesh.
[2] Department of Materials Science and Engineering (MSEN), Texas A&M University, College Station, United States.

**ARTICLE INFO**

***Article history:***
Received 31 August 2023
Received in revised form 10 October 2023
Accepted 30 October 2023
Available online 30 November 2023

**ABSTRACT**

In this study, three samples were created using gravity die casting, i.e., two models of immiscible alloys, Alloy 1 (Al-12wt.%Sn-8wt.%Cu) and Alloy 2 (Al-20wt.%Sn-10wt.%Cu), along with a control sample of pure Al. These gravity die-cast samples, homogenized at 700 ℃ for 2 hours, are analyzed for mechanical properties and microstructures. Optical microscopy and scanning electron microscopy with energy dispersive spectroscopy (EDS) were used to analyze the changes in the Al-Sn-Cu solidified system resulting from the addition of specific alloying elements. Both Alloy 1 and Alloy 2 showed better mechanical properties than the control sample of pure Al. The tensile strength of Alloy 2 shows a decrease from 110.878 MPa to 105.750 MPa compared to Alloy 1. However, there is an increase in the yield strength from 30.239 MPa to 32.362 MPa when the addition of tin exceeds 12% and copper exceeds 8%, respectively, which might be because of the alpha-phase solid solution's interdendritic region that produces lattice strains. The impact resistance and ductility of the alloy are compromised as the hardness increases with the addition of more alloying elements. Alloy 2 exhibited the highest hardness at 50.92 HB. The Brinell hardness values suggest these alloys are potential candidates to replace antifriction bronzes. However, hard CuAl2 is produced at the grain boundaries when copper percentages are increased, reducing the impact properties. The effects of different alloying constituents and melt treatment on the microstructural control of Al-Sn-Cu solidified alloy were also studied. The aluminum matrix with a semi-continuous network (reticular) distribution of tin on the grain boundary was observed. The grain size gradually decreased from 19.65 µm to 16.94 µm and became more equiaxed for Al-20wt.%Sn-10wt.%Cu than Al-12wt.%Sn-8wt.%Cu. The bond between tin and matrix improved with the increasing alloying element. The data obtained from this experiment will undoubtedly contribute to future research in this field.

***Keywords:***
Gravity Die Casting, Al-Sn-Cu System, Mechanical Properties, Microstructure, EDS Analysis

* *Corresponding author.*
*E-mail address:* khansharme@gmail.com (Razia Khan Sharme)
*E-mail of co-authors:* mahinczs@gmail.com, ibeborhan@gmail.com, salmanhaque@mse.kuet.ac.bd, fahimkhanprionto@tamu.edu

https://doi.org/10.37934/mjcsm.12.1.84101

## 1. Introduction

Aluminum-based alloys have a wide range of applications as bearing materials and anti-reflective coatings [1]. The durability and textural properties of these alloys are well-balanced. They are gaining popularity in various industries due to their outstanding mechanical, tribological, physical, and surface properties, surpassing those of their base alloys. These properties include high mechanical strength, better resistance to wear and seizure, better high-temperature properties, precise control of thermal expansion coefficients, and high conductivity [2-4]. These properties are obtained through a combination of methods, including the addition of alloy elements, cold working, and heat treatment processes. Among these, one of the practised processes in metallurgy is selecting alloying elements based on their suitability and impact.

Adding new elements to enhance tensile properties, corrosion resistance, and other desirable characteristics has been a significant advancement over the past century [5]. Increasing the amount of alloying elements generally improves the overall performance of the alloy [6]. The effects of alloying, such as major elements (Si, Cu, Mg), minor elements (Ni, Sn), microstructure modifier elements (Ti, B, Sr, Be, Mn, Cr), and impurity elements (Fe, Zn), on the microstructures and mechanical properties of aluminum alloys have been studied in the past [8]. Adding copper to aluminum alloys, enhances their mechanical properties and structural features, influencing aluminum's precipitation behavior during age-hardening treatments and ultimately leading to increased strength [9]. Additionally, copper creates a protective oxide layer that helps to prevent corrosion [10]. As the melting temperature of copper (1085 °C) is higher than aluminum (660.3 °C), alloying copper with aluminum increases the heat resistivity of the alloy and thus can be used in applications where high heat resistance is required, such as automotive parts or aerospace components [11]. Copper is also a highly conductive material, so alloying copper in aluminum will increase the overall conductivity, which can be useful in electrical and electronic applications [12]. However, adding a large amount of alloying elements such as Zn, Mg, and Cu to improve performance will also cause the alloy's elongation to be reduced and microstructure defects to occur [13]. On the other hand, tin (Sn), a non-toxic and safe material, is commonly used in aluminum casting alloys to reduce friction in bearing and bushing applications [14]. In emergency situations, adding tin as an alloying element can provide temporary liquid lubrication to rubbing surfaces if these bearings or bushings overheat excessively during service [15]. Because of its anti-welding solid qualities with iron, Sn is required in bearing applications, providing adequate surface properties [16].

When copper and tin are added to the aluminum system, they produce ternary-based alloys. Ternary Al-Sn-Cu-based alloys are renowned for their outstanding tribological, mechanical, and physical properties [17-19]. A review of the ternary Al-Sn-Cu system is discussed by Mirković *et al.* [20], where a combination of the CALPHAD (CALculation of PHAse Diagrams) thermodynamic modeling technique, DSC experimental tests, and microstructural analysis was used to investigate the complicated features of the Al-Sn-Cu phase diagram, which are dominated by ternary liquid de-mixing. The CALPHAD method is a practical approach for creating thermodynamic and property databases. This technique involves extrapolating descriptions of binary and ternary systems to calculate data for higher-order systems, resulting in the generation of databases that accurately model complex systems in an efficient manner [21]. It was also demonstrated how seemingly minor alloy composition changes might result in dramatically diverse microstructures. However, most research currently in this field is based on simulations and lacks significant experimental evidence. There is a noticeable gap in the body of work when it comes to empirical research on alloying pure aluminum. The existing experimental research on adding Cu and Sn independently to aluminum alloy has laid a foundation, but there is still room for further exploration and innovation by observing the

effects of adding Cu and Sn together to pure aluminum. Our research in this domain aims to explore the changes in the behavior of pure aluminum by utilizing alloying elements and also to investigate the potential application from their characteristics obtained.

This study aims to investigate the consequences of Cu and Sn addition on the microstructure and mechanical properties of the Al-Sn-Cu system. The samples were fabricated using the gravity die-casting method, and subsequent mechanical tests were performed on the solidified alloy. The microstructural analysis was done using Optical Microscopy (OM) and Scanning Electron Microscope (SEM). After that, the elemental analysis was carried out by EDS. The variations in the mentioned properties were meticulously observed as the amount of alloying components increased, which will help us identify the potential place for its use.

## 2. Methodology

Abed [22] has reported that adding up to 20% Sn to aluminum alloy increases the overall strength and improves microstructural properties. These outcomes align with a similar study conducted by Forrester. These enhanced properties reduce friction and provide temporary liquid lubrication to overheating bearings and bushings [23]. However, it's worth noting that adding 40% tin to the material decreased tensile strength and increased brittleness, according to Abed's study [22]. Conversely, copper also plays a significant role in increasing the strength and hardness of aluminum casting alloys. It also improves the machinability of alloys by increasing matrix hardness [24]. On the downside, it's essential to acknowledge that copper generally reduces the corrosion resistance of aluminum. In specific alloy compositions and tempers, increased copper content can lead to greater susceptibility to stress corrosion [25-27]. Therefore, it is crucial to carefully moderate the percentage of copper in the alloy to strike a balance between strength and minimizing stress corrosion susceptibility. Considering these factors, we carefully selected the percentages of Sn and Cu to optimize mechanical strength and other crucial properties in our research. A locally available Al bar was used as the primary matrix for conducting the gravity die casting. Sn and Cu powder particles of commercial purity were used as alloying elements. However, the experimental procedure can be categorized into the following major areas: (i) Preparing the alloy samples, (ii) Mechanical Tests, and (iii) Microstructural Analysis.

### *2.1 Preparing the alloy samples*

Three samples were made with a gravity die-casting process. The amount of raw materials used for each sample is listed in Table 1. The aluminum gravity die-casting method began with the creation of a mold. The permanent mold was preheated at 200 °C to improve mould filling and reduce thermal shock. The raw materials of aluminum were melted into a liquid state in a gas-fired refractory ceramic crucible with the gravity-casting machinery. It was heated to around 700 °C to homogenize the melt and kept for 2 hours. The molten aluminum was poured into permanent molds to fill the cavity so that it could take the shape of the cavity when it solidified. The necessary alloying weight percentages were added and stirred to the liquid aluminum to ensure homogenized alloying. Copper was melted first, and aluminum was added since copper has a higher melting temperature than aluminum. Tin, which has the lowest melting temperature, was melted last. Each sample was homogenized for 1 hour and then cooled in air to attain the characteristics of an extruded alloy. Finally, the aluminum gravity die-casting removed blanks from the mold.

**Table 1**
Composition of Samples

| Sample | Al (gm) | Sn (gm) | Cu (gm) |
|---|---|---|---|
| Control Sample | 435 | 0 | 0 |
| Alloy 1 | 348 | 142 | 118 |
| Alloy 2 | 305 | 236 | 145 |

The crucible was emptied and cleaned after each melt to prevent contamination. It was ensured that the workplace was free from dust, dirt, or foreign particles and there were no residues from previous melting that could introduce impurities. Some additional raw materials were added to compensate for that loss to mitigate the potential loss of raw materials through vaporization during the heating process, thereby ensuring accuracy. The casting temperature was also properly maintained using temperature monitoring and control systems to prevent excessive oxidation and impurity absorption. Upon completion of the elimination of the flash, all necessary post-processing procedures, such as shot blasting and machining, were executed. Initially, the excess materials were removed from the surface for the machining. Then, finally, the shaping, improving, and finishing of the cast product to meet the required specifications and surface quality were done during the machining process in aluminum gravity die casting. The prepared samples are listed in Table 2.

**Table 2**
List of Samples

| Sample No. | Percentage (%) of Al | Percentage (%) of Sn | Percentage (%) of Cu |
|---|---|---|---|
| Control Sample | 100 | 0 | 0 |
| Alloy 1 | 80 | 12 | 8 |
| Alloy 2 | 70 | 20 | 10 |

### *2.2 Mechanical Properties Test*

Tensile strength, yield strength, ductility, impact resistance, hardness, and fracture toughness are all determined via mechanical characteristics testing. Some of the most important mechanical tests were done to evaluate the properties of the gravity die-cast samples.

#### *2.2.1 Tensile Test*

The tensile testing specimens were fabricated according to ASTM International Standards ASTM E-8M. All the specimens were 50 mm in gauge length and 12.5 mm in diameter. The cross-section of all the samples was 122.719 $mm^2$. A computerized universal testing machine, the Tinius Olsen (TUE-C-400), was used to perform the test at a crosshead speed of 0.5 mm/min and a maximum load rating of 25 KN. Figure 1 shows the specimen during the tensile testing.

#### *2.2.2 Brinell Hardness Test*

The hardness tests for all the samples were conducted utilizing a Brinell hardness tester. The specimen was machined according to ASTM International Standards ASTM E18-22. The specimen had a diameter of 12.5 mm and a height of 30 mm. The grinding machine was used to make the samples smooth for the hardness test, as shown in Figure 2(a). The machine was fitted with a 10 mm diameter intender (hardened steel ball) and a 600 kgf load, and 12 s dwell time was employed to ensure

accurate results. Figure 2(b) shows the sample during the hardness test. The hardness was measured on a B scale.

**Fig. 1.** Tensile test in progress

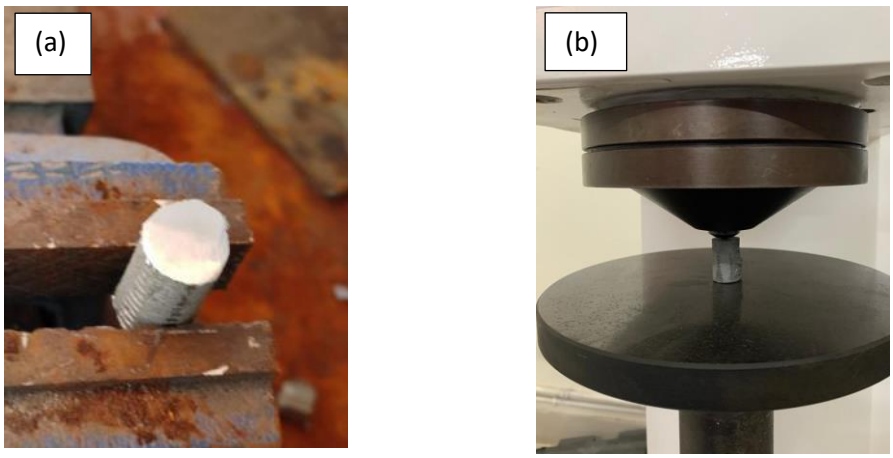


**Fig. 2.** Hardness test specimen (a) After grinding and (b) During hardness test

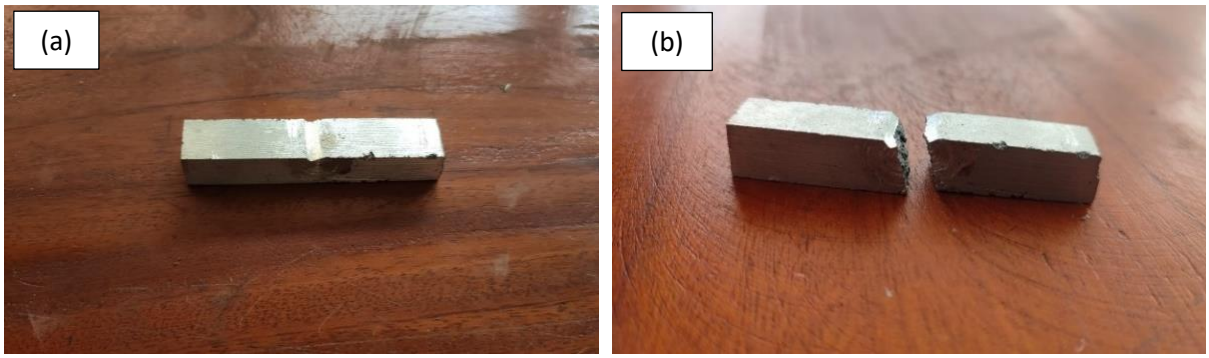


**Fig. 3.** V-notch Impact test specimen (a) Before the impact test (b) The fractured surface after impact test

### *2.2.3 Impact Testing*

The impact test was carried out using the Impact Testing Machine (Charpy): AIT-300-ASTM. The specimens for testing the impact tests were prepared according to ASTM International standards (ASTM-E-23). Figure 3(a) represents the sample before the test was performed. The sample's

dimensions are 55 mm x 10 mm x 10 mm with a 2 mm notch at the centre. The pendulum was raised to the left until it reached its maximum energy range on the upper indicator unit to test the energy range of the specimen. The maximum scale graduation of the machine was 300 Joules (Charpy). The maximum weight of the pendulum was 22.35 kg. The length of the pendulum was 775 mm. The pendulum dropping angle was 140 degrees. Next, the specimen was placed horizontally across supports, with the notch facing away from the pendulum. The pendulum was released, and the value indicated on the indicator unit was recorded. After the test, the brake was applied to return the pendulum to its stable vertical position. The specimen was removed from the testing area, and the failure surface was observed, as displayed in Figure 3(b).

### *2.3 Microstructure Analysis*

The samples were sequentially ground with emery paper of grit 150, 220, 400, 550, 800, 1000, 1200, and 1500 microns in succession. While changing from one emery paper to another, the direction was rotated by 90 degrees. After grinding the surface, the sample was polished using diamond paste made of aluminum oxide and machine oil, followed by a thorough rinse. Subsequently, it was etched for 20 seconds using Kellar's solution and then cleaned with acetone. Finally, the prepared sample was ready for placement in the Amscope optical microscope. Various images were taken at different magnifications using the optical microscope. The samples underwent a gold coating process to prepare them for SEM imaging. Afterwards, SEM images were captured using JEOL JCM-7000 NeoScope benchtop SEM operated at 5 kV. Additionally, the SEM was linked with the EDS attachment for comprehensive analysis.

## 3. Results

### *3.1 Mechanical Properties*

#### *3.1.1 Tensile Test Results*

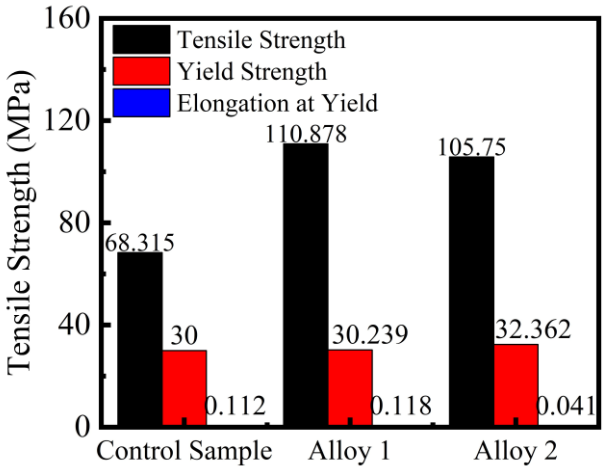


**Fig. 4.** Comparison of tensile properties of the alloys

Figure 4 depicts the changes in the tensile test performance of the samples. The yield strength for the control sample is 30 MPa, while it is 30.239 MPa and 32.362 MPa for Alloy 1 and Alloy 2, respectively. So, the yield strength improved slightly with increasing alloying elements in the control

sample. This may be attributed to the creation of lattice strains and impediments that restrict the free movement of dislocations [28].

Furthermore, the control sample has a tensile strength of 68.315 MPa, while Alloy 1 exhibits the highest tensile strength at 110.878 MPa, and Alloy 2 has a strength of 105.750 MPa. The tensile strength initially increased with the addition of Sn and Cu in the control sample but then decreased as the alloying percentages increased. The reason behind the initial rise in tensile strength of Alloy 1, as compared to the control sample, can be attributed to the incorporation of foreign atoms like Sn and Cu in the lattice. This addition makes it difficult for dislocations to move, leading to the formation of solid solutions. However, an increase in the percentage of added alloying elements led to decreased tensile strength, as seen in Alloy 2. A similar result is found in another study where Reddy *et al.* [29] reported that the tensile strength of alloys with 10% Cu percent is lower than that of alloys with 5% Cu concentration. This is due to the higher phase in the alpha-phase solid solution's interdendritic region [29]. Because of this reason, the interstitial spaces in the system might get occupied by Sn or Cu. As a result, the regularity of the aluminum lattice structure gets disrupted, and overall tensile strength decreases.

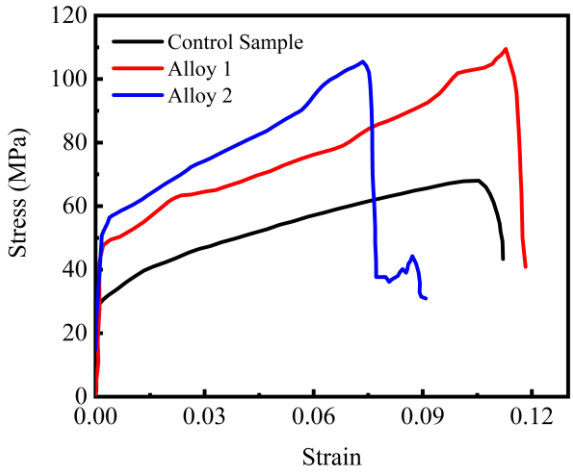


**Fig.5.** Engineering stress-strain curves of pure Al and its alloys

Figure 5 displays the stress-strain curves for the control sample and the alloys. Alloy 2 exhibits superior elastic properties among the alloys due to its higher yield stress than the other alloys. Meanwhile, Alloy 1 can handle more considerable stresses before necking because of its greater ultimate tensile strength. On the other hand, pure aluminum has the lowest ultimate tensile strength of the three samples, with a measurement of 68.316 MPa. The difference between yield and ultimate strengths implies that there is a lower occurrence of strain hardening in pure aluminum compared to the two alloys.

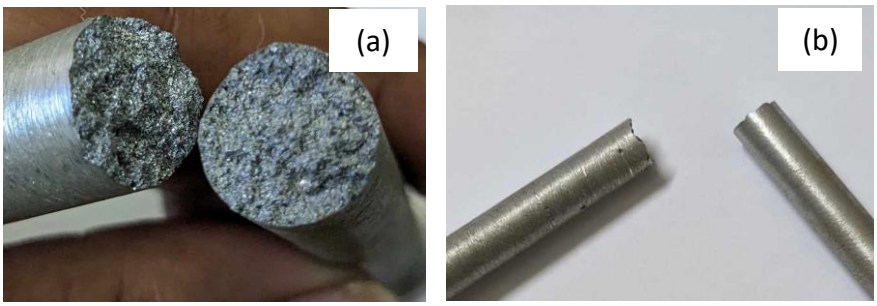


**Fig. 6.** Fracture surface of the control sample (Pure Al) after tensile test: (a) top view, (b) side view

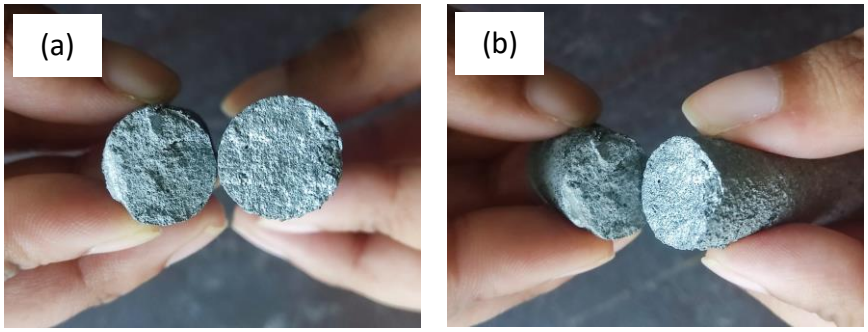


**Fig. 7.** Fracture surface after tensile test for (a) Alloy 1 (Al-12wt.%Sn-8wt.%Cu) and (b) Alloy 2 (Al-20wt.%Sn-10wt.%Cu)

In Figure 6, the fracture surfaces display ductile fracture after the tensile test of the control sample. Figure 7 shows the impact of adding alloying elements, with alloy 1 and alloy 2 indicating a gradual shift towards an almost brittle fracture surface. Sn and Cu alloys have the potential to combine to generate intermetallic compounds like Al-Sn [30], $Cu_3Sn$ [31], and θ-$Al_2Cu$ [32, 33]. The initiation and spread of cracks might result from the production of these intermetallic phases, lowering the alloy's overall strength.

### *3.1.2 Hardness Test Results*

Table 3 depicts the comparison among the three samples. The hardness gradually increased for Alloy 1 and Alloy 2 with the increasing alloying percentages. This is due to precipitation hardening. The $Al_2Cu$ precipitate creates a metastable phase, which significantly increases the hardness [34]. The hardness exceeds 20 HB in both of the cases with adding alloying elements (Cu, Sn). As a result, it can offer potential Al-based bearing materials that could take the place of antifriction bronzes [35].

**Table 3**
Hardness results

| Samples | Diameter of indentation, d | BHN= $\frac{2P}{\pi D[D-\sqrt{D^2-d^2}]}$ (HB) |
|---|---|---|
| Control Sample | 5.1 mm | 28 |
| Alloy 1 | 4.3 mm | 39.31 |
| Alloy 2 | 3.8 mm. | 50.92 |

The Brinell hardness value was calculated from the Eq. 1 and summarized in Table 3. The unit is in the B scale for hardness.

$$BHN= \frac{2P}{\pi D[D-\sqrt{D^2-d^2}]} \quad (1)$$

where, D = Ball Diameter (mm), P = Load applied (kg-f), d = Diameter of indentation (mm).

### *3.1.3 Impact Test Results*

Charpy impact energy values indicate a material's resistance to sudden force [36]. Figure 8 shows the Charpy impact test results for all three samples. The impact strength of a material is typically determined by measuring the amount of energy it absorbs when it fractures. The control sample has the highest absorbed energy with an impact strength of 352 KJ/$m^2$. The impact strength gradually decreased with adding alloying percentages to the pure Al.

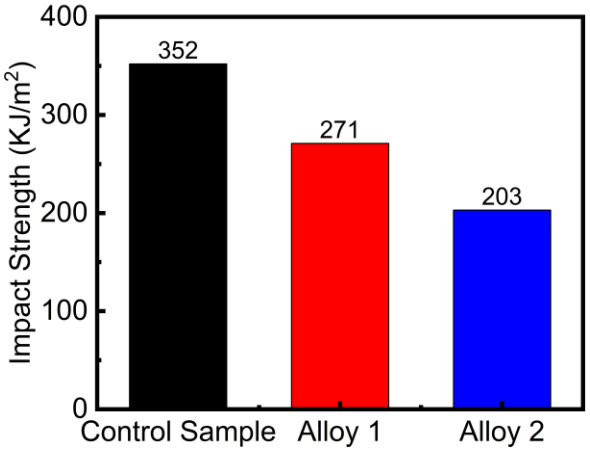


**Fig. 8.** Impact strength of the samples

Alloy 2 exhibited a substantial 42.33% decrease compared to the control sample. While adding Cu and Sn to pure aluminum increased hardness, it also rendered the alloy more brittle. This caused a reduction in plastic deformation energy, which increased the likelihood of debonding during fractures and decreased impact strength [37]. Aluminum alloys have more plastic deformation energy, but as the material becomes less brittle, the plastic deformation energy decreases, reducing impact strength. When aluminum alloys become less ductile, stress concentration areas increase, which promotes crack formation and propagation. These cracks can cause debonding and decrease impact strength. Samal *et al.* [37] and Kumar *et al.* [38] have reported similar results by adding a percentage of TiC and reinforcing fly ash in aluminum alloy. However, the addition of brittle fly ash particles has led to a reduction in the toughness of the aluminum alloy. Adeosun *et al.* [32] have investigated that copper additions greater than 4% reduced UTS, elongation, and impact energy. In this study, as Cu addition increased above 4 vol% in both of the alloys, the presence of hard $CuAl_2$ at grain boundaries caused a loss in overall ductile properties and an increase in hardness. However, the strength reduction may be caused by tin particles in the lattice.

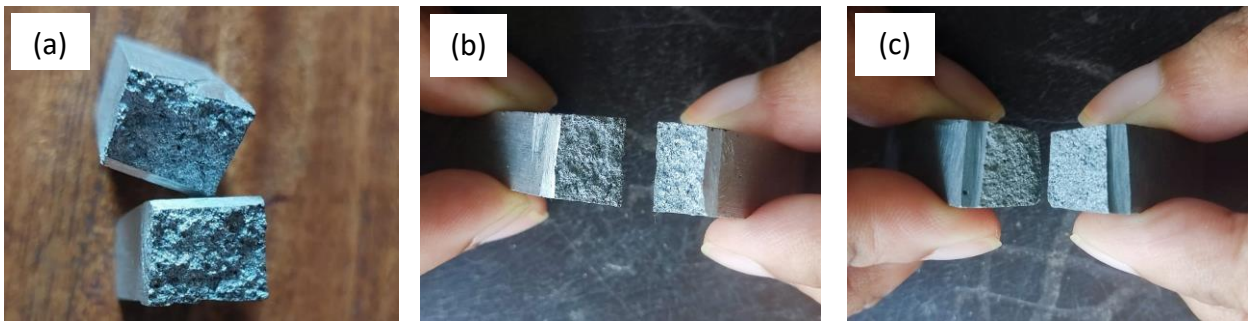


**Fig. 9.** Visual observation of fracture surfaces after impact test for (a) Control sample (Pure Al), (b) Alloy 1 (Al-12wt.%Sn-8wt.%Cu), and (c) Alloy 2 (Al-20wt.%Sn-10wt.%Cu)

Fracture surfaces of the Charpy impact specimens of pure Al and the alloys are presented in Figure 9. A higher percentage of tin (Sn) content contributes to increasing brittleness by promoting the formation of intermetallic brittle phases and making them more susceptible to cracking. As a result, with the alloying percentage, the surface turns to more prone to brittle fractures.

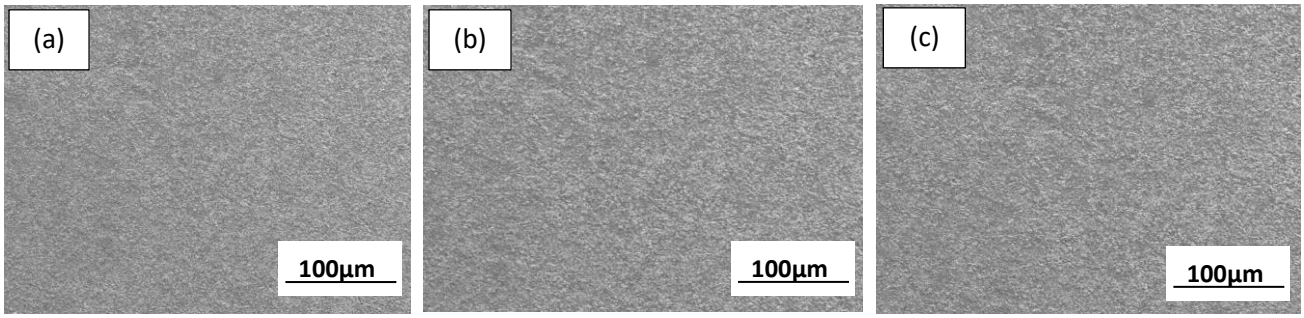


**Fig. 10.** Optical microscopic view of (a) Control sample (Pure Al), (b) Alloy 1 (Al-12wt.%Sn-8wt.%Cu), and (c) Alloy 2 (Al-20wt.%Sn-10wt.%Cu)

Figure 10 shows the optical microscopic view of the fracture surfaces after Charpy impact testing. The microstructures clearly reveal a flat and uniform appearance across all three samples, indicating the surface's brittle fracture mode.

### *3.2 Microstructural Evaluation*

Microstructural analysis was performed on all three samples using optical and scanning electron microscopy and energy dispersive spectrometry.

#### *3.2.1 Optical Microstructural Analysis*

Figure 11 shows the optical microscopic view of pure aluminum with indistinct grains and some visible pores. The strength of metal comes from its crystal lattice grains, while the areas between them are weaker. This interplay creates aluminum's unique properties. Because of the indistinct grains, it does not show higher strength and high ductility.

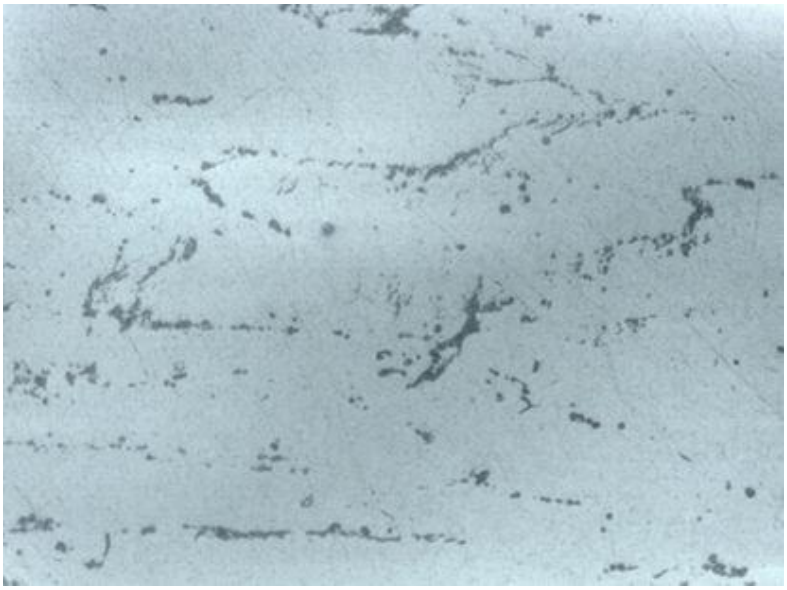

**Fig. 11.** Optical micrographs of the control sample (pure Al) at 200X magnifications

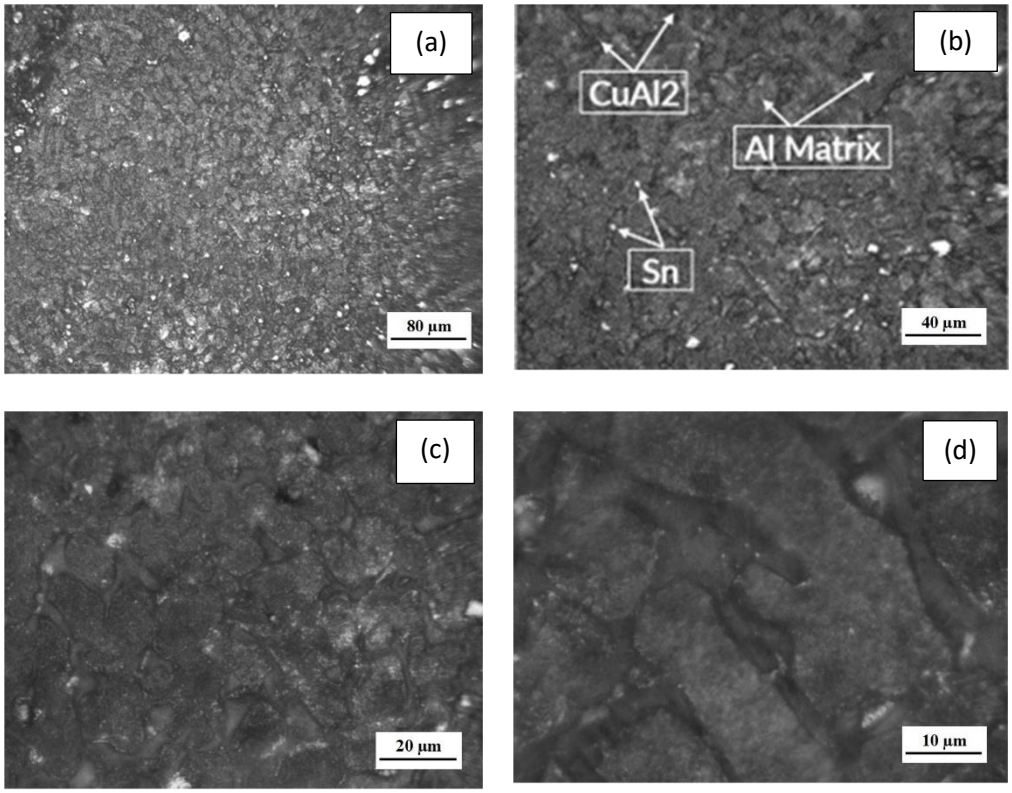


**Fig. 12.** Optical micrographs of Alloy 1 (Al-12Sn-8Cu) at (a)50X, (b) 100X, (c)200X, and (d) 400X magnifications

Figure 12 shows the microstructural image for different resolutions for Alloy 1, where we can see the isolated Sn phase with Cu particle distribution. We can also see that Al-12Sn-8Cu exhibited equiaxed Al grains, while Sn was found in two forms: globular precipitates evenly distributed among Al grains and irregularly shaped particles at grain boundaries. Since similar investigation was done by Wang *et al.* [39], where it was noted that with the addition of Sn to the deposits in their as-deposited state substantially improved the microstructure, and the grains were changed. Wang *et al.* [39] also showed that the grains converted to equiaxed crystals from dendrites, and the size of the equiaxed crystals was approximately 30 µm. The resolvable Sn phase increased as 8wt% Cu was added to this alloy. The Sn phase can be seen at the intersplat boundaries and within the elongated splats. We can also see an aluminum matrix with a semi-continuous network (reticular) distribution of tin on the grain boundary.

Figure 13 shows the optical microstructures for Alloy 2 at different magnifications. As the percentages of Sn and Cu increase, the changes in the microstructure can clearly be seen in Figure 13. The grains are changed for Sn in the Al matrix with Cu precipitation. The grain size reduction can be seen for tin along the grain boundaries. In a similar study, Kurz [40] stated that with the addition of 5% Cu to the Al-Sn alloy, the thickness of the tin film crystallized around primary aluminum decreased, and the size of the tin particles was lowered by interfering with the Ostwald ripening process. The hard $Al_2Cu$ intermetallic phase is well dispersed in the interdendritic portions of these samples, which feature refined microstructures with small dendritic spacings. Optical microscope findings demonstrate that as the weight percentages of the Al-Sn-Cu alloy change, the Sn particles coarsen to a lower degree near the intersplat boundary.

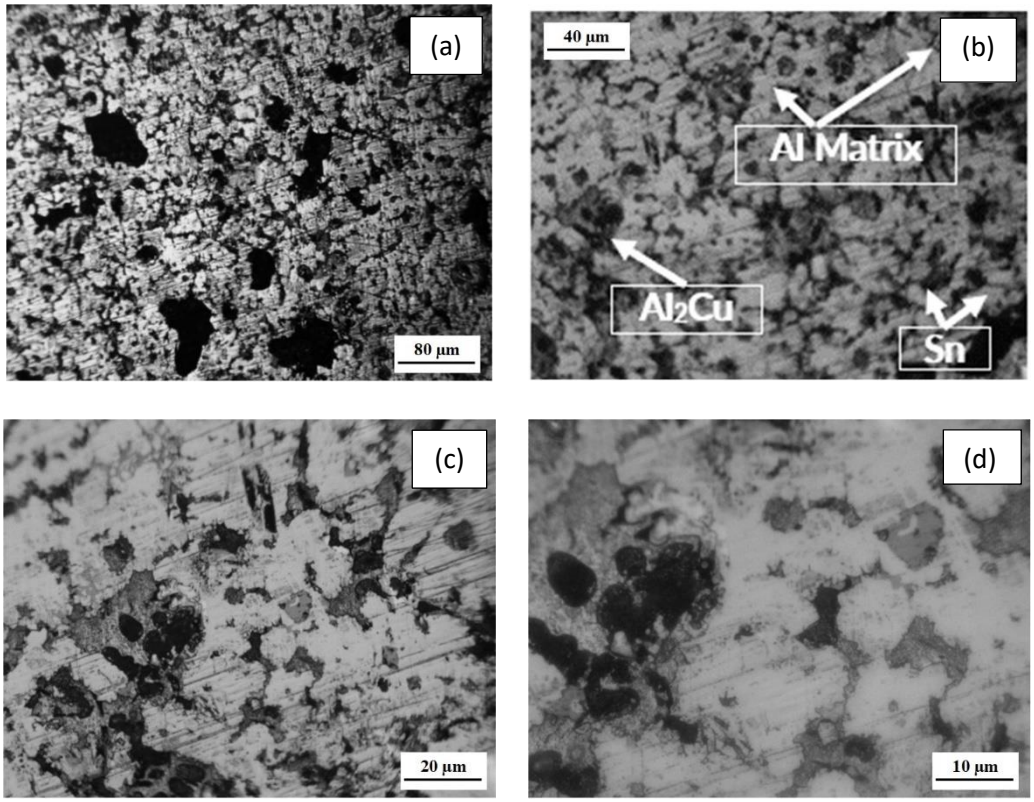


**Fig. 13.** Optical micrographs of Alloy 2 (Al-20Sn-10Cu) at (a)100X, (b) 200X, (c)400X, and (d) 1000X magnifications

### *3.2.2 SEM-EDS analysis*

Figure 14 shows the SEM imaging of pure aluminum. Microstructural investigations in scanning electron linked with an energy dispersive spectrometry attachment showed the structure of pure Al. It has been observed in Figure 11 that the microstructure does not consist of different phases. This observation is confirmed by EDS analysis, which reveals two peak sets, as seen in Figure 14(b). The presence of dark areas in both SEM and OM images can be attributed to over-etching and surface oxidation, indicating the presence of oxygen. The presence of gold can be observed using EDS due to the gold coating.

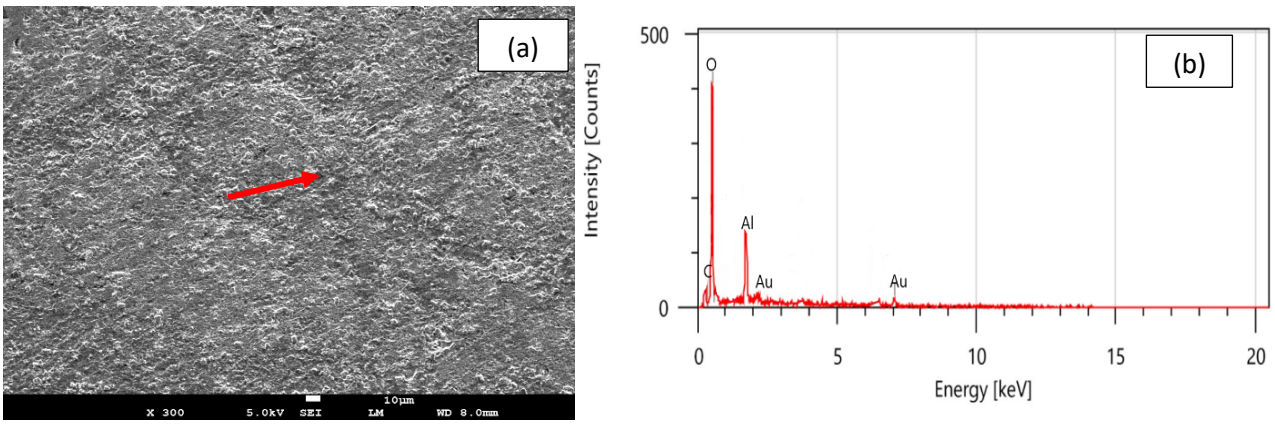


**Fig. 14.** (a) SEM image and (b) EDS analysis in the marked region of pure aluminum

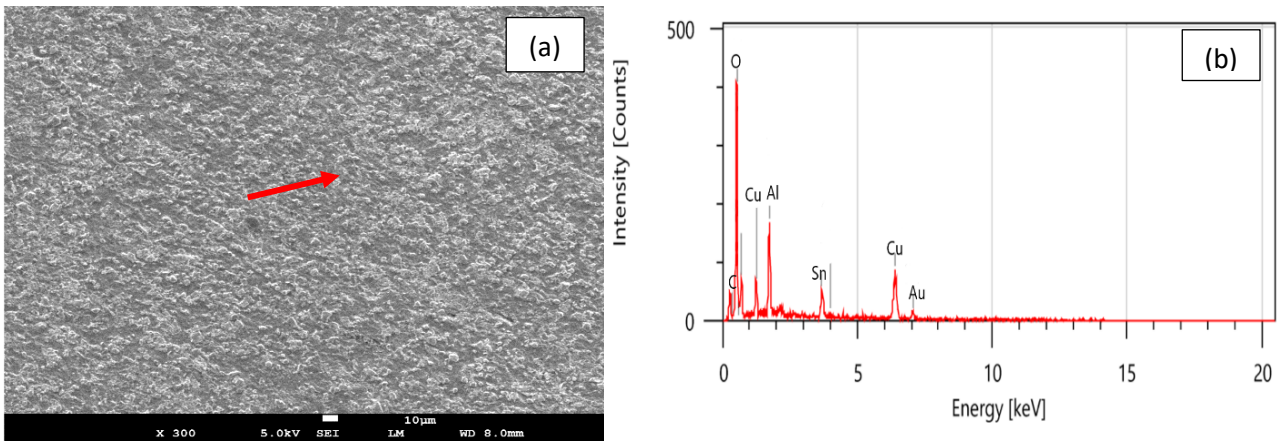


**Fig. 15.** (a) SEM image and (b) EDS analysis in the marked region of Alloy 1

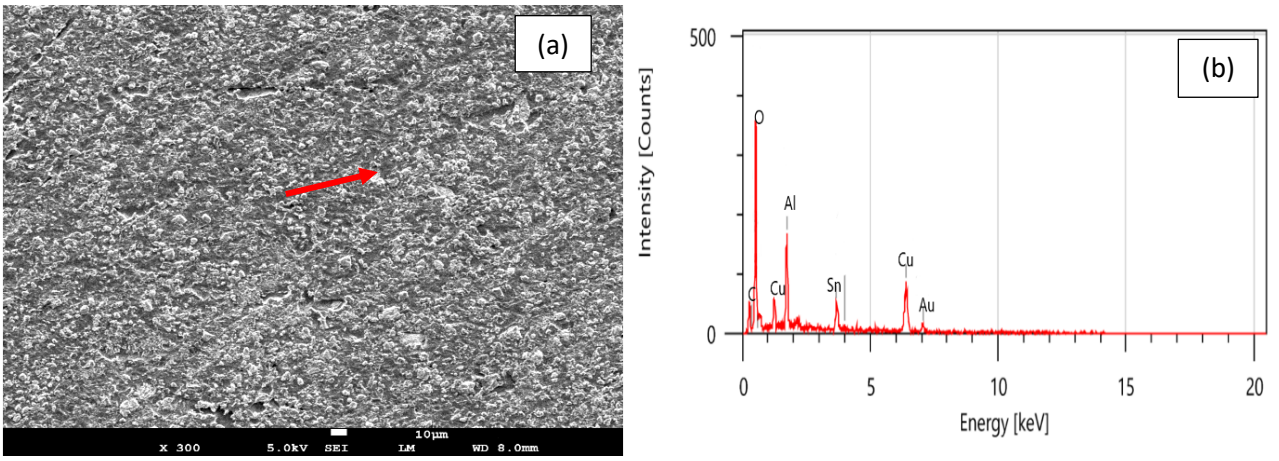


**Fig. 16.** (a) SEM image and (b) EDS analysis in the marked region of Alloy 2

Figures 15 and 16 show the SEM images and EDS analyses for Alloy 1 and Alloy 2, respectively. Notably, the grain structure becomes finer with an increasing concentration of alloying elements, rendering exceptional strength for these alloys. Specifically, Figures 15(b) and 16(b) show that the Al-matrix contains Sn and Cu, as detected by EDS. In both cases, the oxidation is indicated by the presence of oxygen. A minor carbon peak is evident, which suggests that there is some presence of surface contamination during sample preparation. However, no other impurities were detected in the EDS analysis of samples. The presence of both Sn and Cu in the Al-matrix suggests the formation of intermetallic compounds in the grain boundaries.

### *3.2.3 Grain size measurement*

Table 4 depicts the average grain sizes of the two alloys. ImageJ software was used to measure grain size. The calculations for the measuring grain size were done by inserting the microstructural image. The average grain size was measured after taking three lines for grain size measurement for both alloys. The average grain size was calculated from the Eq. 2 and summarized in Table 4. All the grains were calculated in micrometers.

$$Average\ grain\ size = \frac{Line\ length}{No.\ of\ grains} \tag{2}$$

**Table 4**

Grain size measurements

| Samples | Line length | | | Average grain size |
|---|---|---|---|---|
| | 1st | 2nd | 3rd | |
| Alloy 1 | 19.62 | 19.69 | 19.65 | 19.65 µm |
| Alloy 2 | 16.92 | 16.97 | 16.94 | 16.94 µm |

As Cu and Sn are introduced to the alloy system, the grain size becomes finer, and the number of grains increases, as shown in Figure 17. As a result, the grain size decreased. In aluminum alloys, Sn and Cu can function as grain refiners.

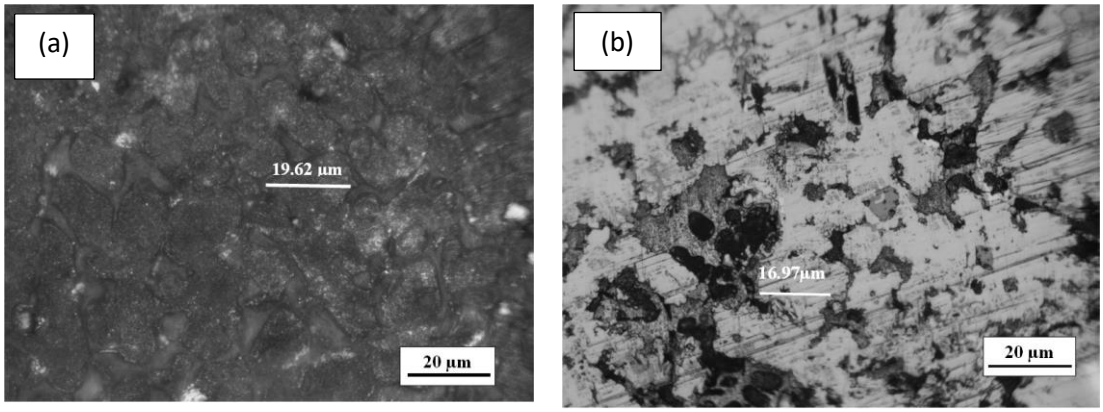


**Fig. 17.** A single grain size of (a) Al-12Sn-8Cu alloy and (b) Al-20Sn-10Cu alloy at 200x

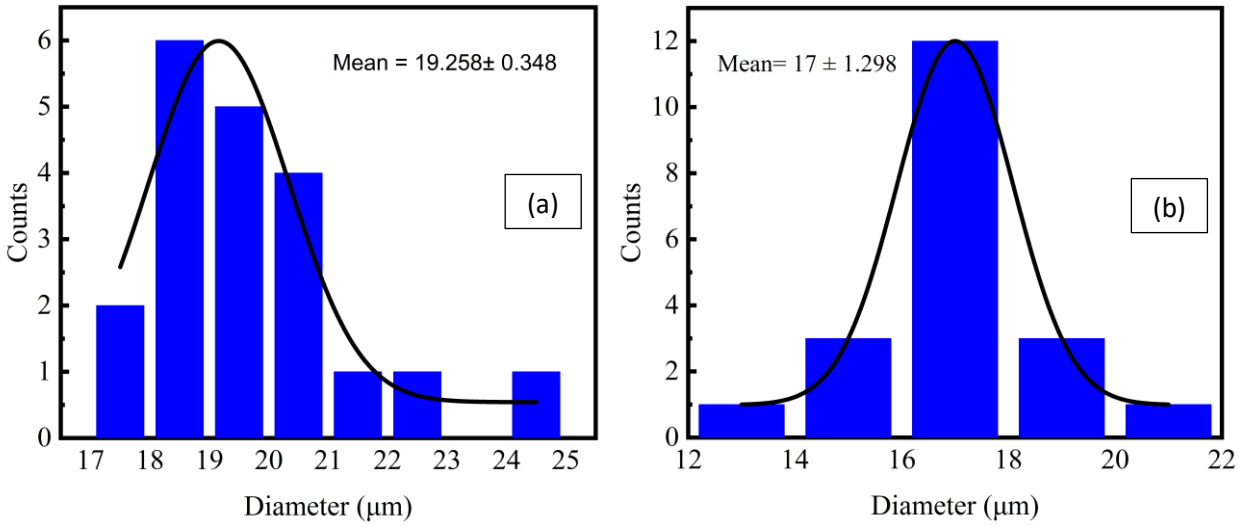


**Fig. 18.** ImageJ grain distribution for (a) Al-12Sn-8Cu alloy and (b) Al-20Sn-10Cu

Figure 18 shows the grain distribution as obtained using ImageJ. The histograms show coherency with the average grain size of the alloys. During solidification, the addition of alloying components promotes the formation of small and uniform equiaxed grains, which can hinder grain expansion and encourage the development of a refined microstructure. The grain size impacts significant mechanical properties like ductility, strength, toughness, fatigue resistance, hardness, etc. Higher strength typically results from smaller grain sizes as more grain boundaries function as barriers to the passage of dislocations. The dislocations travel less before coming into contact with a grain boundary, increasing the material's strength and resistance to deformation, reducing ductility, and increasing

hardness. Higher toughness is typically the result of finer grain sizes since more grain boundaries can assist in dispersing energy and stopping crack development.

## 4. Conclusions

The research aims to find Al-Sn-Cu solidified alloy's mechanical and microstructural properties by changing the alloying compositions to help guide further assessment in various applications. The mechanical and microstructural properties change when alloying elements are added in succession. Sn and Cu are added to the base alloy of pure Al, at 12% and 20% for the former, and 8% and 10% for the latter, to observe or predict the characteristics of the alloys. This study has revealed some significant results, as listed below:

1. Adding Cu and Sn to pure Al significantly improves its mechanical properties. However, the tensile test result has revealed that the yield strength is higher in Alloy-2 (Al-20wt.%Sn-10wt.%Cu) than Alloy-1 (Al-12wt.%Sn-8wt.%Cu), whereas the tensile strength is higher in Alloy-1 (Al-12wt.%Sn-8wt.%Cu) than Alloy-2 (Al-20wt.%Sn-10wt.%Cu). This is because the Sn and Cu alloys have the potential to combine to generate intermetallic compounds like Al-Sn, $Cu_3Sn$, and θ-$Al_2Cu$, which may cause strains.
2. The hardness is increased for Al-20wt.%Sn-10wt.%Cu compared to Al-12wt.%Sn-8wt.%Cu due to precipitation hardening.
3. The addition of the alloying element to the control sample reduced impact strength, as indicated by the Charpy impact test results. This can be attributed to the presence of $CuAl_2$, a hard intermetallic phase, and brittle phases at the grain boundaries. As a result, the impact resistance and ductility of the alloy are compromised while its hardness is increased.
4. Microstructural evolution for adding Sn and Cu in the Al matrix has shown changed grain size. The grain size is reduced for Alloy 2, where the percentage of Cu is higher. The grains for pure Al are indistinctive. More defined and bright images are found in Alloy 2 than in Alloy 1. The segregation of tin is much lower in Alloy 1 than Alloy 2. $CuAl_2$ phase fine particles were observed. The grain size is decreased for Al-20wt.%Sn-10wt.%Cu alloy than for Al-12wt.%Sn-8wt.%Cu alloy.

## Acknowledgment

The authors would like to express their gratitude to everyone who contributed to the completion of this study at the Department of Materials Science & Engineering, Khulna University of Engineering & Technology, Khulna, Bangladesh.

## References

[1] Q.M. Mehran, M.A. Fazal, A.R. Bushroa and S. Rubaiee, "A Critical Review on Physical Vapor Deposition Coatings Applied on Different Engine Components," Critical Reviews in Solid State and Materials Sciences 43, no. 2 (2018): 158-175. https://doi.org/10.1080/10408436.2017.1320648

[2] E.O. Ezugwu, J. Bonney and Y. Yamane, "An Overview of the Machinability of Aeroengine Alloys," Journal of Materials Processing Technology 134, no. 2 (2003): 233-253. https://doi.org/10.1016/S0924-0136(02)01042-7

[3] P.D. Srivyas and M.S. Charoo, "Role of Reinforcements on the Mechanical and Tribological Behavior of Aluminum Metal Matrix Composites–A Review," Materials Today: Proceedings 5, no. 9 (2018): 20041-20053. https://doi.org/10.1016/j.matpr.2018.06.371

[4] D. Sarkar, R.K. Sharme and F. Khan. "A Study on the Tensile Properties from the Composition of an Annealed Structural Steel Sample" *International Conference on Mechanical Engineering and Renewable Energy*, Chittagong University of Engineering & Technology (CUET), Bangladesh, December 12-14, 2021.
[5] W. Melik, Z. Boumerzoug and F. Delaunois, "Characterization of the Al6061 Alloy Reinforced with SiC Nanoparticles and Prepared via Powder Metallurgy," Malaysian Journal on Composites Science and Manufacturing 9, no. 1 (2022): 22-34.
https://doi.org/10.37934/mjcsm.9.1.2234
[6] B. Mingo, R. Arrabal, M. Mohedano, C.L. Mendis, R. Del Olmo, E. Matykina, N. Hort, M.C. Merino and A. Pardo, "Corrosion of Mg-9Al Alloy with Minor Alloying Elements (Mn, Nd, Ca, Y and Sn)," Materials & Design 130, (2017): 48-58.
https://doi.org/10.1016/j.matdes.2017.05.048
[7] F. Khan and H.M.M.A Rashed. "Phase Transformation in Micro-Alloyed Steels," *in Engineering Steels and High Entropy-Alloys*, ed. A. Sharma, Z. Duriagina, S. Kumar (London, IntechOpen, 2020): 39-44 https://www.intechopen.com/chapters/72244
[8] N.A.H. Hasim, S. Akmal, S.K. Sayed Nordin, R.H. Hambali, M.F. Mamat, A.T.J.A. Alshamsi and S. Pawenang, "Modelling Total Quality Management in the Malaysian Composite Manufacturing Industry," Malaysian Journal on Composites Science and Manufacturing 7, no. 1 (2022): 11-22.
https://doi.org/10.37934/mjcsm.7.1.1122
[9] T.C. Chang, J.Y. Wang, C.L. Chu and S. Lee, "Mechanical Properties and Microstructures of Various Mg–Li Alloys," Materials Letters 60, no. 27 (2006): 3272-3276.
https://doi.org/10.1016/j.matlet.2006.03.052
[10] B. Trachli, M. Keddam, H. Takenouti and A. Srhiri, "Protective Effect of Electropolymerized 3-Amino 1, 2, 4-Triazole Towards Corrosion of Copper in 0.5 M NaCl," Corrosion Science 44, no. 5 (2002): 997-1008.
https://doi.org/10.1016/S0010-938X(01)00124-X
[11] H.R. Kotadia, E. Doernberg, J.B. Patel, Z. Fan and R. Schmid-Fetzer, "Solidification of Al-Sn-Cu Based Immiscible Alloys Under Intense Shearing," Metallurgical and Materials Transactions A 40, (2009): 2202-2211.
https://doi.org/10.1007/s11661-009-9918-x
[12] Chunqi Yu, Yicheng Feng, Lei Wang, Jinlai Fu, Fuwei Kang, Sicong Zhao, Erjun Guo and Baoxia Ma, "Effect of Pre-Stretching Deformation Treatment Process on Microstructure and Mechanical Properties of Al-Cu-Mg Alloy," Materials Today Communications 31, (2022): 103368.
https://doi.org/10.1016/0927-796X(95)00180-8
[13] Y. Xu, Z. Zhang, Z. Gao, Y. Bai, P. Zhao and W. Mao, "Effect of Main Elements (Zn, Mg and Cu) on the Microstructure, Castability and Mechanical Properties of 7xxx Series Aluminum Alloys with Zr and Sc," Materials Characterization 182 (2021): 111559.
https://doi.org/10.1016/j.matchar.2021.111559
[14] F. Khan, S. Mondal, H.M. Usama, A. Sharif and M.A. Matin, "Synthesis and Characterization of Ba2+, La3+, Zr4+ Co-Modified Multiferroic BiFeO3," In IOP Conference Series: Materials Science and Engineering, vol. 438, no. 1, p. 012031. IOP Publishing, 2018.
https://doi.org/10.1088/1757-899X/438/1/012031
[15] L. Guo, P. Zuo, Z. Zhang, Q. Zhang, M. Zhao, X. Hou, J. Wu and B. Zhang, "A Review of Cu–Ni–Sn Alloys: Processing, Microstructure, Properties, and Developing Trends," Materials 16, no. 1 (2023): 444.
https://doi.org/10.3390/ma16010444
[16] F. Meydaneri, B. Saatçi and M. Özdemir, "Thermal Conductivities of Solid and Liquid Phases for Pure Al, Pure Sn and Their Binary Alloys," Fluid Phase Equilibria 298, no. 1 (2010): 97-105.
https://doi.org/10.1016/j.fluid.2010.07.015
[17] L. Ratke and S. Diefenbach, "Liquid Immiscible Alloys," Materials Science and Engineering: R: Reports 15, no. 7-8 (1995): 263-347.
https://doi.org/10.1016/0927-796X(95)00180-8
[18] M. Xu, Y.G. Yin, C.M. Li and C.C Duan, "A Comparative Study on Sn Macrosegregation Behavior of Ternary Al-Sn-Cu Alloys Prepared by Gravity Casting and Squeeze Casting," China Foundry 20, no. 1 (2023): 63-70.
https://doi.org/10.1007/s41230-023-2046-1
[19] Subodh K. Das, J. A. S. Green and J. Gilbert Kaufman, "The Development of Recycle-Friendly Automotive Aluminum Alloys," Jom 59 (2007): 47-51.
https://doi.org/10.1007/s11837-007-0140-2
[20] D. Mirković, J. Gröbner and R. Schmid-Fetzer, "Liquid Demixing and Microstructure Formation in Ternary Al–Sn–Cu Alloys," Materials Science and Engineering: A 487, no. 1-2 (2008): 456-467.
https://doi.org/10.1016/j.msea.2007.10.043

[21] S. Bigdeli and M. Selleby, "A Thermodynamic Assessment of the Binary Fe-Mn System for the Third Generation of Calphad Databases," Calphad 64 (2019): 185-195.
https://doi.org/10.1016/j.calphad.2018.11.011
[22] E.J. Abed, "Study of Solidification and Mechanical Properties of Al-Sn Casting Alloys," Asian Trans. Eng 2, no. 3 (2012): 89-98.
[23] S. Das, D.P. Mondal, S. Sawla and N. Ramakrishnan, "Synergic Effect of Reinforcement and Heat Treatment on the Two Body Abrasive Wear of an Al–Si Alloy Under Varying Loads and Abrasive Sizes," Wear 264, no. 1-2 (2008): pp. 47–59.
https://doi.org/10.1016/j.wear.2007.01.039
[24] M. Tash, F.H. Samuel, F. Mucciardi and H.W. Doty, "Effect of Metallurgical Parameters on the Hardness and Microstructural Characterization of As-Cast and Heat-Treated 356 and 319 Aluminum Alloys," Materials Science and Engineering: A 443, no. 1-2 (2007): 185-201.
https://doi.org/10.1016/j.msea.2006.08.054
[25] M.O. Speidel, "Stress Corrosion Cracking of Aluminum Alloys," Metallurgical Transactions A 6 (1975): 631-651.
https://doi.org/10.1007/BF02672284
[26] P.P.N.K.V. Rambabu, N. Eswara Prasad, V.V. Kutumbarao and R.J.H. Wanhill, "Aluminium Alloys for Aerospace Applications," Aerospace Materials and Material Technologies: Volume 1: Aerospace Materials (2017): 29-52.
https://doi.org/10.1007/978-981-10-2134-3_2
[27] T. Dursun and C. Soutis, "Recent Developments in Advanced Aircraft Aluminium Alloys," Materials & Design (1980-2015) 56 (2014): 862-871.
https://doi.org/10.1016/j.matdes.2013.12.002
[28] B. J. Brindley and P. J. Worthington, "Yield-Point Phenomena in Substitutional Alloys," Metallurgical Reviews 15, no. 1 (1970): 101-114.
https://doi.org/10.1179/mtlr.1970.15.1.101
[29] T.B. Reddy, P. Karthik and M.G. Krishna, "Mechanical Behavior of Al–Cu Binary Alloy System/Cu Particulates Reinforced Metal-Metal Composites," Results in Engineering 4 (2019): 100046.
https://doi.org/10.1016/j.rineng.2019.100046
[30] P. Bassani, M. Molteni and E. Gariboldi, "Microstructural Features and Thermal Response of Granulated Al and A356 Alloy with Relevant Sn Additions," Materials & Design 229 (2023): 111879.
https://doi.org/10.1016/j.matdes.2023.111879
[31] Encyclopedia Copper Development Association Inc., s.v. "Copper-Tin Intermetallic Compounds," accessed October 2, 2023.
https://copper.org/applications/industrial/DesignGuide/performance/coppertin03.php
[32] S.O. Adeosun, S.A. Balogun, L.O. Osoba, W.A. Ayoola and A.M. Oladoye, "Effect of Cu and Zn Addition on the Mechanical Properties of Structural Aluminum Alloy," Journal of Modern Manufacturing Technology 3, no. 1 (2011): 103-110
https://ir.unilag.edu.ng/handle/123456789/8218
[33] W.S. Ebhota and T.C. Jen, "Intermetallics Formation and Their Effect on Mechanical Properties of Al-Si-X Alloys," Intermetallic Compounds-Formation and Applications (2018): 21-41.
http://dx.doi.org/10.5772/intechopen.73188
[34] S. Bahl, L. Xiong, L.F. Allard, R.A. Michi, J.D. Poplawsky, A.C. Chuang, D. Singh, T.R. Watkins, D. Shin, J.A. Haynes and A. Shyam, "Aging Behavior and Strengthening Mechanisms of Coarsening Resistant Metastable θ'precipitates in an Al–Cu Alloy," Materials & Design 198 (2021): 109378.
https://doi.org/10.1016/j.matdes.2020.109378
[35] N.A. Belov, T.K. Akopyan, I.S. Gershman, O.O. Stolyarova and A.O. Yakovleva, "Effect of Si and Cu Additions on the Phase Composition, Microstructure and Properties of Al-Sn Alloys," Journal of Alloys and Compounds 695 (2017): 2730-2739.
https://doi.org/10.1016/j.jallcom.2016.11.193
[36] P.K. Jena, K.S. Kumar, R.K. Mandal and A.K. Singh, "An Experimental Study on the Fracture Behavior of Different Aluminium Alloys Subjected to Ballistic Impact," Procedia Structural Integrity 17 (2019): 957-964.
https://doi.org/10.1016/j.prostr.2019.08.127
[37] P. Samal, P.R. Vundavilli, A. Meher and M.M. Mahapatra, "Recent Progress in Aluminum Metal Matrix Composites: A Review on Processing, Mechanical and Wear Properties," Journal of Manufacturing Processes 59 (2020): 131-152.
https://doi.org/10.1016/j.jmapro.2020.09.010

[38] K.R. Kumar, K.M. Mohanasundaram, R. Subramanian and B. Anandavel, "Influence of Fly Ash Particles on Tensile and Impact Behaviour of Aluminium (Al/3Cu/8.5 Si) Metal Matrix Composites," Science and Engineering of Composite Materials 21, no. 2 (2014): 181-189.
https://doi.org/10.1515/secm-2013-0006

[39] Shuai Wang, HuiMin Gu, Wei Wang, ChengDe Li, Ling Ling Ren, Zhen Biao Wang, YuChun Zhai and PeiHua Ma, "Effect of Sn Content on the Microstructure and Properties of Wire and Arc Additive Manufactured Al-Cu Alloy Deposits," 3D Printing and Additive Manufacturing 7, no. 1 (2020): 28-36.
https://doi.org/10.1089/3dp.2019.0176

[40] W. Kurz, M. Rappaz and R. Trivedi, "Progress in Modelling Solidification Microstructures in Metals and Alloys. Part II: Dendrites from 2001 to 2018," International Materials Reviews 66, no. 1 (2021): 30-76.
https://doi.org/10.1080/09506608.2020.1757894